Vector field mapping of local polarization using gold nanoparticle functionalized tips: independence of the tip shape

K. G. Lee[1], H. W. Kihm[1], K. J. Ahn[1], J. S. Ahn[1], Y. D. Suh[2], C. Lienau[3], and D. S. Kim[1*]

[1]*Department of Physics and Astronomy, Seoul National University, Seoul 151-747, Korea*
[2]*Korea Research Institute of Chemical Technology 107, Yuseong-Gu, Daejeon 305-600, Korea*
[3]*Carl von Ossietzky Universität Oldenburg, Institut für Physik, D-26111 Oldenburg, Germany*
**Corresponding author: dsk@phya.snu.ac.kr*

Abstract: We have measured local electric field vectors of local polarizaton on the nanoscale using gold nanoparticle functionalized tips as local field scatterers. In our experiments, the local field induces a dipole-moment in the gold nanoparticle functionalized tip, which then radiates into the far-field, transferring the full information about the local electric field from the near into the far field. The polarization characteristics of the scattered fields are analyzed using a conventional ellipsometry method. The tip dependent scattering function- the polarizability tensor- is fully determined by far field scattering measurements. Once the polarizability tensor for each tip is correctly accounted for in the data analysis, our results show that the finally determined local field polarization vectors are essentially independent of the tip shape.

OCIS codes: (120.5820) Scattering measurements; (260. 2130) Ellipsometry and polarimetry; (260.5430) Polarization

References and links

1 A. Lewis, M. Isaacson, A. Harootunian, and A. Muray, "Development of a 500 Å spatial resolution light microscope," Ultramicroscopy **13**, 227-231 (1984). http://www.sciencedirect.com/science?_ob=ArticleListURL&_method=list&_ArticleListID=593399642&_sort=d&view=c&_acct=C000013398&_version=1&_urlVersion=0&_userid=198559&md5=7d957a939b269ad26d465d7bd6adc0b3

2 D. W. Pohl, W. Denk, and M. Lanz, "Optical stethoscopy: image recording with resolution λ/20," Appl. Phys. Lett. **44,** 651-653 (1984). http://scitation.aip.org/getabs/servlet/GetabsServlet?prog=normal&id=APPLAB000044000007000651000001&idtype=cvips&gifs=yes

3 E. Betzig, J. K. Trautman, J. S. Weiner, T. D. Harris, and R. Wolfe, "Polarization contrast in near-field scanning optical microscopy," Appl. Opt. **22,** 4563 (1992). http://ao.osa.org/abstract.cfm?id=40089

4 F. Zenhausern, M. P. O'Boyle, and H. K. Wickramasinghe, "Apertureless near-field optical microscope," Appl. Phys. Lett. **65,** 1623-1625 (1994). http://scitation.aip.org/getabs/servlet/GetabsServlet?prog=normal&id=APPLAB000065000013001623000001&idtype=cvips&gifs=yes

5 Y. Inouye and S. Kawata, "Near-field scanning optical microscope with a metallic probe tip," Opt. Lett. **19** 159-161 (1994). http://ol.osa.org/abstract.cfm?id=12150

6 K. G. Lee, H. W. Kihm, J. E. Kihm, *et al*., "Vector field microscopic imaging of light," Nature Photon. **1**, 53-56 (2007). http://www.nature.com/nphoton/journal/v1/n1/abs/nphoton.2006.37.html

7 H. Chew, D. –S. Wang, and M. Kerker, "Elastic scattering of evanescent electromagnetic waves," Appl. Opt. **18,** 2679 (1979). http://ao.osa.org/abstract.cfm?id=23275

8 G. Videen, "Light scattering from a sphere on or near a surface," J. Opt. Soc. Am. A. **8,** 483 (1991). http://josaa.osa.org/abstract.cfm?id=4011

9 D. Ganic, X. Gan, and M. Gu, "Parametric study of three-dimensional near-field Mie scattering by dielectric particles," Opt. Commun. **216,** 1-10 (2003).

10 D. E. Aspnes, "Foulier transformation detection system for rotating-analyzer ellipsometers," Opt. Commun. **8**, 222-225 (1973).

11 P. S. Hauge and F. H. Dill, "Design and operation of ETA, and Automated Ellipsometer," IBM J. Res. Develop. **17**, 472-489 (1973).

#85586 - $15.00 USD Received 23 Jul 2007; revised 5 Sep 2007; accepted 5 Sep 2007; published 29 Oct 2007

http://domino.watson.ibm.com/tchjr/journalindex.nsf/0b9bc46ed06cbac1852565e6006fe1a0/47d82e1ff4acd49585256bfa006841c4?OpenDocument
12 R. Greef, "An automatic ellipsometer for use in electrochemical investigations," Rev. Sci. Instrum. **41**, 532-538 (1970). http://scitation.aip.org/getabs/servlet/GetabsServlet?prog=normal&id=RSINAK000041000000400053200001&idtype=cvips&gifs=yes
13 M. Born and E. Wolf, *Principles of Optics – 7th ed*. p.25 Eq. 12 (Cambridge University Press, Cambridge, England, 1999).
14 H. F. Hazebroek, and A. A. Holscher, "Interferometric ellipsometry," J. Phys. E: Sci. Instru. **6,** 822-826 (1973). http://www.iop.org/EJ/abstract/0022-3735/6/9/013
15 R. Hillenbrand, F. Keilmann, P. Hanarp, D. S. Sutherland, and J. Aizpurua, "Coherent imaging of nanoscale plasmon patterns with a carbon nanotube optical probe," Appl. Phys. Lett. **83**, 368-370 (2003). http://scitation.aip.org/getabs/servlet/GetabsServlet?prog=normal&id=APPLAB000083000002000368000001&idtype=cvips&gifs=yes
16 R. Dändliker, P. Tortora, L. Vaccaro, and A. Nesci, "Measuring three-dimensional polarization with scanning optical probes," J. Opt. A **6** S18-S23 (2004). http://www.iop.org/EJ/abstract/1464-4258/6/3/003
17 R. M. A. Azzam, "Division-of-amplitude photopolarimeter (DOAP) for the simultaneous measurement of all four Stokes parameters of light," Optica Acta 29, 685-689 (1982). http://www.informaworld.com/smpp/content~content=a713820903~db=all
18 R. M. A. Azzam, "Arrangement of four photodetectors for measuring the state of polarization of light," Opt. Lett. **10,** 309-311 (1985). http://ol.osa.org/abstract.cfm?id=8453
19 T. Kalkbrenner, M. Ramstein, J. Mlynek, and V. Sandoghdar, "A single gold particle as a probe for apertureless scanning near-field optical microscopy," J. Microsc. **202,** 72-76 (2001). http://www.blackwell-synergy.com/doi/full/10.1046/j.1365-2818.2001.00817.x
20 Z. H. Kim, and S. R. Leone, "High-resolution apertureless near-field optical imaging using gold nanosphere probes," J. Phys. Chem.B **110,** 19804-19804 (2006). http://pubs.acs.org/cgi-bin/article.cgi/jpcbfk/2006/110/i40/html/jp061398+.html
21 T. Kalkbrenner, U. Håkanson, and V. Sandoghdar, "Tomographic plasmon spectroscopy of a single gold nanoparticle," Nano Lett. **4,** 2309-2315 (2004). http://pubs.acs.org/cgi-bin/abstract.cgi/nalefd/2004/4/i12/abs/nl048694n.html
22 P. C. Gasson, *Geometry of Spatial Forms-Ch. 8* (John Wiley & Sons, New York, USA, 1983).
23 J. Ellis and A. Dogariu, "Optical polarimetry of random fields," Phys. Rev. Lett. **95,** 203905 (2005). http://scitation.aip.org/getabs/servlet/GetabsServlet?prog=normal&id=PRLTAO000095000020203905000001&idtype=cvips&gifs=Yes

1. Introduction

The orientation of the field vector of local polarizaton is a key quantity in many thousands of theoretical studies on nano-optics, nanophotonic devices and optical sciences in general. The ability to experimentally probe electromagnetic field vectors of local polarization with nanometer resolution is of fundamental importance for understanding essentially all near-field phenomena. While experimental techniques aimed at probing the field intensity, e.g. aperture-based [1, 2] or apertureless [3-5] near-field microscopies, are rapidly improving, the local orientation of the electromagnetic field vector could not be readily accessed experimentally. Recently it was reported that a polarization analyzed detection of light scattered off gold nanoparticle functionalized tips makes it possible to simultaneously determine both the direction and magnitude of the local field [6]. The electric dipole radiation carries the full information about the local electric fields from the near field into the far field region. Gold particle functionalized tips scatter the local fields through the electric dipole radiation when the particle size is small compared to the wavelength of light [7-9]. Because the polarization state of the scattered light is strongly dependent on the scattering function of this dipole scatterer, i.e., its polarizability tensor, it is important to characterize each tip carefully before the local electric field orientation can be reconstructed.

To investigate both experimentally and theoretically how the effect of different tips can be corrected in the final determination of the field vector of local polarizaton, we prepared three tips functionalized with gold nanoparticles of different shapes and sizes. The corresponding polarizability tensor of each of these tips is measured in a far-field scattering experiment. The polarization characteristics of photons scattered by these gold nanoparticle-functionalized tips are then analyzed using the rotational analyzer ellipsometry (RAE) method [10-12]. In our

#85586 - $15.00 USD Received 23 Jul 2007; revised 5 Sep 2007; accepted 5 Sep 2007; published 29 Oct 2007

experiments, the local polarization state of an optical standing wave generated on the prism surface is successfully reconstructed. Within the dipole scattering regime, this reconstruction is independent of the geometrical shape of the tip, provided that its polarization tensor is well known and a back-transformation process is used.

2. Principles and Experimental methods

A general elliptical polarization state of the local electric field at a fixed position $\vec{r}$ in the x-z plane can be written as [13]:

$$\vec{E}_{Local}(\vec{r}) = (E_x, E_z) = (a_1 e^{i\omega t + i\delta_1}, a_2 e^{i\omega t + i\delta_2}), (a_1, a_2 > 0), \quad (1)$$

This field vector rotates at a frequency ω along the perimeter of an ellipse. In our experiments, a dipole scattering tip gives a scattered field $\vec{E}_S \propto \ddot{\alpha} \cdot \vec{E}_{Local}$ where $\ddot{\alpha}$ is the polarizability tensor of the scatterer, which we model in the following as being point-like. Then, the polarization state of the scattered field is determined by the RAE method in which a linear polarizer, mounted inside the optical path of the scattered light and in front of the detector, is rotated by 360° in 10° steps. The detected field intensity passing through a polarizer is then given as

$$I \propto \left\langle \left| \vec{P} \cdot E_S \right|^2 \right\rangle = \left\langle \left| (\cos\varphi \quad \sin\varphi) \ddot{\alpha} \begin{pmatrix} E_{Local,x} \\ E_{Local,z} \end{pmatrix} \right|^2 \right\rangle \quad (2),$$

where φ is the detecting polarizer angle from the x-axis and $\langle ... \rangle$ denotes a time average over many optical cycles.

The polar diagram $\sqrt{I(\varphi)}$ shown in Fig. 1(a), recorded by rotating the polarizer in 10° steps, allows us to determine the polarization state of the scattered light depicted as a red colored ellipse. The major axis angle of the ellipse corresponds to the detecting polarizer angle at which the measured intensity has its maximum and the major and minor axes lengths are proportional to the square-root of the maximum and minimum intensities, respectively. In this way, the shape of the polarization ellipse of the scattered field ($\vec{E}_S$) is reconstructed. The only missing information is the sense of rotation and the absolute phase, i.e., the point on the ellipse at $t = 0$, of the field vector. In principle this additional information about the phase and sense of rotation – which is irrelevant for almost all linear optical experiments - can be determined by applying interferometry [14, 15, 16] and Stokes parameter ellipsometry [17, 18]. One experimental polar diagram $\sqrt{I(\varphi)}$ is explicitly shown in Fig. 1(b): a gold nano-particle functionalized tip sits at a selected position and scatters a standing wave created by two counter-propagating evanescent waves on a prism surface. The corresponding ellipse is denoted in red color. In case of a highly elliptical polarization as in the standing wave which is our main interest in this paper, we denote this ellipse with a double arrowed linear vector (red arrow) for a better visualization. Finally the polarization state of the local field $\vec{E}_{Local}$ is then reconstructed by a back-transformation $\ddot{\alpha}^{-1} \cdot \vec{E}_S$ (black arrow).

#85586 - $15.00 USD Received 23 Jul 2007; revised 5 Sep 2007; accepted 5 Sep 2007; published 29 Oct 2007

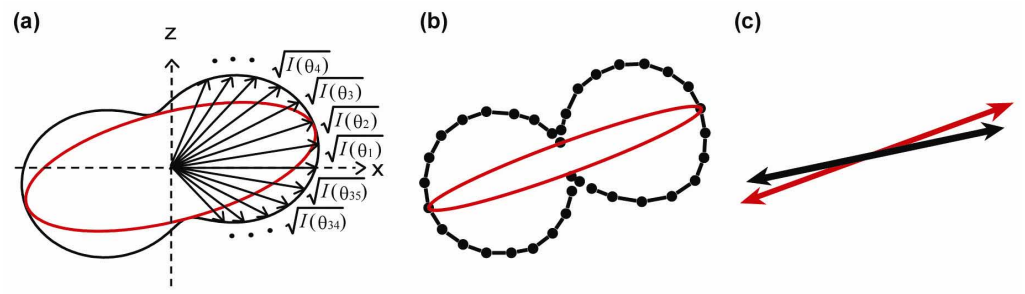

Fig. 1. Schematics of the experimental procedure. (a) The outer-plot (black line) results from a polar plot of the squared-rooted intensities for every detecting polarizer angle. The angle (θ_{max}) of the measured intensity maximum corresponds to the major axis angle and the square-rooted maximum (minimum) intensity is proportional to the major (minor) axis length. (b) One such experimental polar plot of the scattered light at one selected position is shown as filled circles. The black line is a guide to the eye. The elliptical polarization state is reconstructed (inner red line). (c) The red arrow represents the long axis of the ellipse shown in (b). By back-transformation using the experimentally determined polarizability tensor of the scatterer, the local field vector of local polarization is determined (black arrow).

We used gold nanoparticle functionalized tips as the local field scatterer [19]. Bare glass optical fiber (FS-SN-4224, Thorlabs) is etched in hydrofluoric acid (49%), and then dipped in 3'-aminopropyltrimethoxysilane (APTES) solution for 10 minutes to generate an adhesive layer to attach gold particles. This tip is scanned across a slide glass or a prism surface where gold nanoparticle solution was spread and dried until eventually a gold particle sticks to the tip end. Generally there is a morphological distribution in commercially treated colloidal gold particles and a slight deformation of the particle shape can be expected in the attachment process [20]. Therefore, the particle shape generally can be considered as an arbitrarily oriented ellipsoid. As long as the electric dipole scattering regime holds, this ellipsoidal scatterer is expressed by three principal axes orthogonal to each other [21]. Since the field direction is determined in an x-z plane of the laboratory frame in this work, we only have to consider the geometric projection of the ellipsoidal scattering function onto the two-dimensional plane, i.e., an ellipse [22].

The scattering function of an arbitrarily oriented ellipse can be traced through polarization-dependent tip characterization [21]. With a defined as the length ratio between the major and the minor principal axes and ζ as the angle between the major axis of the scatterer and the laboratory frame x-axis, the polarizability tensor can be written as

$$\ddot{\alpha} = \begin{pmatrix} \cos\zeta & -\sin\zeta \\ \sin\zeta & \cos\zeta \end{pmatrix} \begin{pmatrix} a & 0 \\ 0 & 1 \end{pmatrix} \begin{pmatrix} \cos\zeta & \sin\zeta \\ -\sin\zeta & \cos\zeta \end{pmatrix} \qquad (3).$$

The polarizability tensor of a tip is experimentally determined in the far-field scattering measurement depicted in Fig. 2(a). The tip end is illuminated by a 780 nm plane wave and the incident beam polarization is rotated using a λ/2 plate. The scattered light is detected in the forward scattering geometry by rotating a linear polarizer in front of an avalanche photo diode (C-4777-01, Hamamatsu) at every incoming beam polarization [Fig. 2(b)]. The polarization tensor is then obtained by fitting the outer rim of the polar plots by an ellipse [Fig. 2(c)]: in the tip shown here, a=1.36 and ζ=6°, so that in the laboratory frame, it can be written as: $\ddot{p} = \begin{pmatrix} 1.35 & 0.036 \\ 0.036 & 1 \end{pmatrix}$. For a good dipole scatterer, this time consuming measurement can be replaced by rotating the incident beam polarization without placing a linear polarizer in the detection part [21]. This simplified measurement generally gives a different shape polar plot compared to the outer rim fitting of the polar plots changing the detecting polarizer angle [Fig.

#85586 - $15.00 USD Received 23 Jul 2007; revised 5 Sep 2007; accepted 5 Sep 2007; published 29 Oct 2007

2(c)]. But in case of a dipole scatterer the two different measurements touch the same four positions: two end points of the major axis and two end points of the minor axis, enabling us to determine the values of a and ζ. The simplified method does, however, assume a-priori knowledge about the dipole nature of the scatterer. We applied both methods for tip characterization and found the results to be consistent with each other.

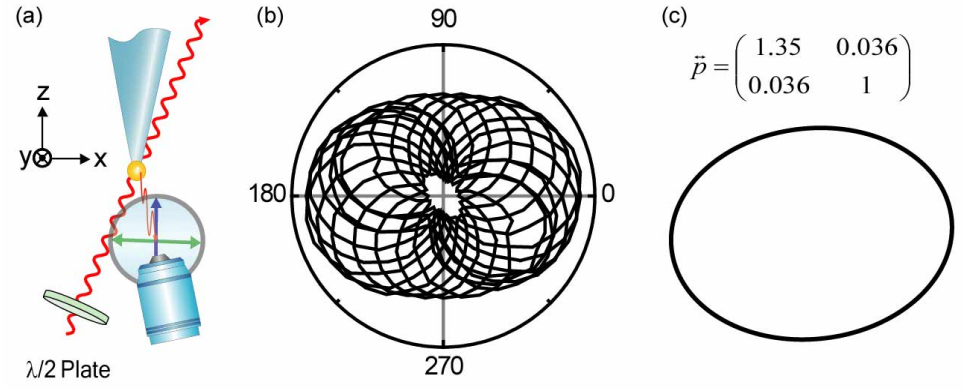

Fig. 2. (a). Schematic diagram of the tip polarizability tensor measurements. The tip end is illuminated by focusing a 780 nm plane wave and the incident beam polarization is rotated by 360° using a λ/2 plate. The tip axis is oriented along the z-axis and the laser beam is incident along the y-axis. The scattered light is detected in the direction of the incident beam by rotating a linear polarizer in front of the detector. (b) Polar plot of the square-rooted intensity of light scattered off the tip end for every incident light polarization. (c) The outer rim of (b) is fitted as an ellipse and the corresponding polarizability tensor is shown in upper part.

Using these gold nanoparticle functionalized tips we measured the polarization state of a standing wave generated on a prism surface. Our experimental setup is schematically depicted in Fig. 3(a). A *p*-polarized plane wave is guided into a prism and generates, with its reflected wave from the mirror at the other side of the prism, an evanescent standing wave on the prism surface, if the incident angle θ_i is set to be larger than the total internal reflection angle $\theta_c = \sin^{-1}\left(n_{air} / n_{prism}\right)$ given by the refractive indices of two media. In Fig. 3(b), theoretically calculated horizontal and vertical field intensities, $|E_x|^2$ and $|E_z|^2$, respectively, of this evanescent standing wave are presented with the corresponding field vectors of polarization shown in the upper part. For an incident angle of θ_i=60° and n_{prism}=1.51 at λ=780 nm, the peak vertical field intensity is about 2.25 times larger than its horizontal counterpart, and these two field components are spatially displaced with a 90° shift in their intensity profiles. We scanned the prism surface along the x-direction and detected the scattered light intensity by rotating the detecting polarizer in 10° steps at every scan position. The tip to sample distance was controlled to be constant using a shear force mode feedback system and the detection angle was set about 20° from the prism surface (–y axis) due to the experimental restrictions. The effects of the detection angle from the surface on the image contrast are beyond the scope of this work and will be discussed elsewhere.

#85586 - $15.00 USD Received 23 Jul 2007; revised 5 Sep 2007; accepted 5 Sep 2007; published 29 Oct 2007

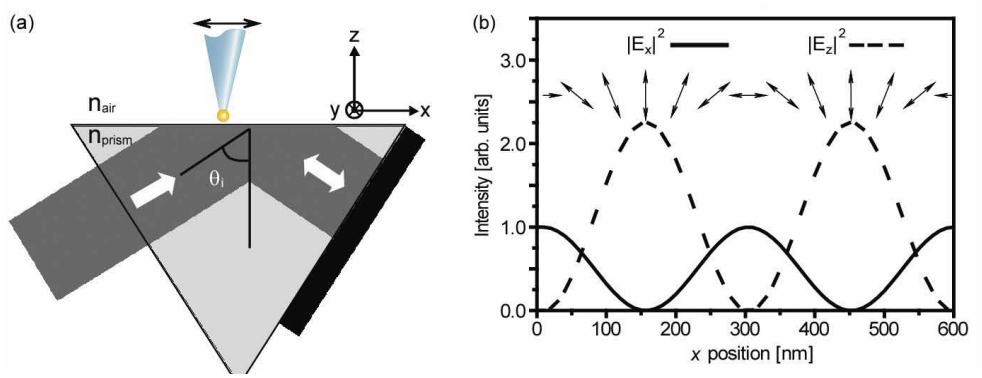

Fig. 3. (a). Experimental setup: A 780 nm cw-mode Ti:Sapphire laser enters at normal incidence into one side facet of an equilaterally shaped prism and is retro-reflected at the other side facet to generate an evanescent standing wave on the top surface. The gold nanoparticle functionalized tip scatters the local fields into far-field region. The detection angle was set about 20° from the prism surface (–y axis). (b) Theoretically calculated local field components as a function of the scatterer position: vertical $|E_z|^2$ (dashed line) and horizontal $|E_x|^2$ (solid line) component, respectively. The corresponding local field vectors of polarization are presented at every position.

3. Results

We prepared three tips functionalized with gold nanoparticles of different size and shape. Figure 4(a) shows, for instance, a scanning electron microscopic image of one of the etched glass fiber tips functionalized with a nominally 200 nm-diameter gold nanoparticle. Figure 4(b) shows the tip characterization results. Lines with filled-squares and open-circles are the polar plots of the square-rooted intensities for the vertical and the horizontal illuminating beam polarizations respectively. These two peanut shaped polar plots clearly support that this tip is indeed well represented by a dipole scatterer. A slight deviation of the long axes of the two polar plots from the corresponding illumination beam polarization directions means that the polarizability tensor has non-diagonal components. Therefore we need to repeat these measurements for all incident beam polarization directions to fully characterize the tensor elements as mentioned in the previous section. The polarization tensor is then obtained by fitting the outer rim of such polar plots by an ellipse. The solid line in Fig. 4(b) shows the polar plot of the square-rooted total intensity measured by rotating the incident beam polarization by 360° with 10° steps, without placing a linear polarizer in the detection part. From this result, we can determine the values α=1.08 and ζ=80° and obtain the polarizability tensor $\ddot{\alpha} = \begin{pmatrix} 1 & 0.014 \\ 0.014 & 1.075 \end{pmatrix}$ using Eq. (3). With this tip which has an almost isotropic scattering function, we scanned the prism surface in the x-direction by rotating the detector polarizer at every scan position. Open circles and filled squares in Fig. 4(c) show the dependence of the scattered field intensity on the polarizer angle φ at two selected spatial positions: at x_1 $\left|E_{S,x}\right|^2$ has a maximum, whereas at x_2 position $\left|E_{S,z}\right|^2$ is maximum respectively. Intensity maxima at x_1 are located at detector polarizer angles $\varphi \approx 0$, π, and 2π, and $\varphi \approx \pi/2$ and $3\pi/2$ at x_2. This shows that the long axes of the polar plot of the square-rooted scattered light intensity are aligned along the x- and z-axis at the positions of x_1 and x_2 respectively, as shown in the upper part in Fig. 4(c). Here, we can see that the two field components of the scattered light are almost out of phase as in the local vector field on the prism surface, and this is expected for this tip with small off diagonal values of the polarizability tensor. The solid lines in Fig. 4(c) are simultaneously fitted to both curves by using Eq. (2). Figure 4(d) shows the

#85586 - $15.00 USD Received 23 Jul 2007; revised 5 Sep 2007; accepted 5 Sep 2007; published 29 Oct 2007

experimentally reconstructed intensity profiles of the horizontal (open-circles) and the vertical (filled-squares) electric field components of the evanescent standing wave within a scanning range of 600 nm. This reconstruction includes the back-transformation using the experimentally measured scattering tensor, We choose the origin as the maximum position of the vertical field component for convenience. The two lines are nearly out of phase as expected from theory, and the ratio between the maxima of the two components is 2.18, which is in good agreement with the calculated value of 2.25.

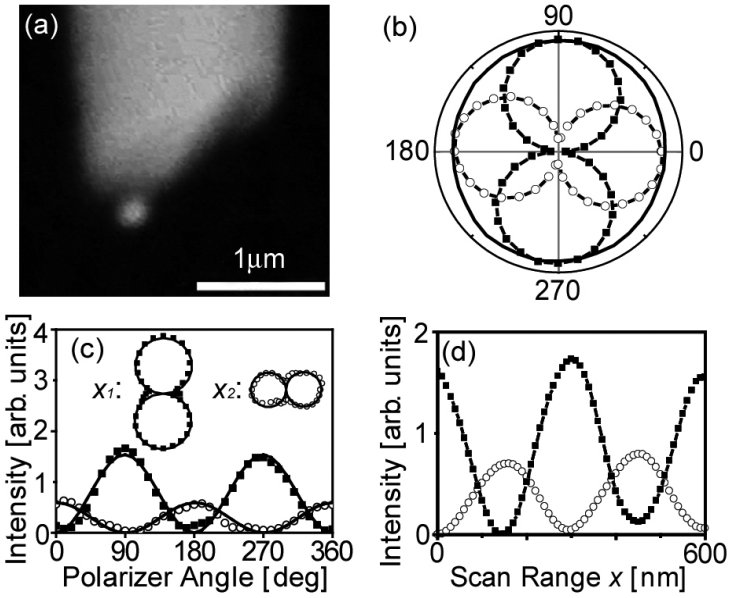

Fig. 4. (a). A SEM image of a gold nanoparticle functionalized tip. (b) Polar plots of the square-rooted intensity of light scattered off the tip end for horizontal (open circles) and vertical (filled squares) polarizations of the incident light, respectively. The solid line represents the polar plot of square-rooted total scattered field intensity by rotating the incident beam polarization by 360° in 10 degrees steps. (c) Dependence of the scattered field intensity on the detecting polarizer angle at position x_1, i.e., for a maximum of $\left|E_{S,x}\right|^2$ (open circles), and at a position x_2, i.e., at a maximum of $\left|E_{S,z}\right|^2$ (filled squares) of the standing wave generated on the prism surface. The solid lines are fitted by using Eq. (2). The upper part shows polar plots generated from the data. (d) Intensity profiles of the field components $E_{Local,x}$ (open circles) and $E_{Local,z}$ (filled squares).

Figure 5(a) shows a far-field characterization result of another gold particle functionalized tip. The solid and the dashed lines are the experimental and fitted data respectively. In this case, the scattering shape is more elongated (a=1.62) and the major axis is positioned at an angle of ζ=33° from the x-axis of the laboratory frame. The off-diagonal terms of the polarizability tensor are relatively large compared with the previous tip. Figure 5(b) shows the scattered field intensity as a function of the detecting polarizer angle at a maximum position of $\left|E_{S,x}\right|^2$ (open circles) and at a maximum position of $\left|E_{S,z}\right|^2$ (filled squares), and solid lines represent a fitting using Eq. (2). This shows a seemingly very different result compared to Fig. 4(c), and suggests that the vector state of the scattered light is considerably modified from that of the local field vector of polarization at these two selected positions. Figure 5(c) shows the spatial intensity profiles for detecting polarizer angles of φ=0° (open circles) and φ =90° (filled squares). The relative phase shift is 67.8° and the maximum

#85586 - $15.00 USD Received 23 Jul 2007; revised 5 Sep 2007; accepted 5 Sep 2007; published 29 Oct 2007

intensity ratio is 1.39. This apparently different result, however, can also be used to recover the correct field vector profile when we apply the back-transformation using the experimentally measured polarizability tensor. The reconstructed local field intensity profiles $E_{Local,x}$ (open circles) and $E_{Local,z}$ (filled squares) are shown [Fig. 5(d)]. The relative phase shift between two field components $\varphi_z - \varphi_x = 83.5°$ and the maximum intensity ratio $I_z/I_x = 2.14$ which almost coincides with the theoretical calculation.

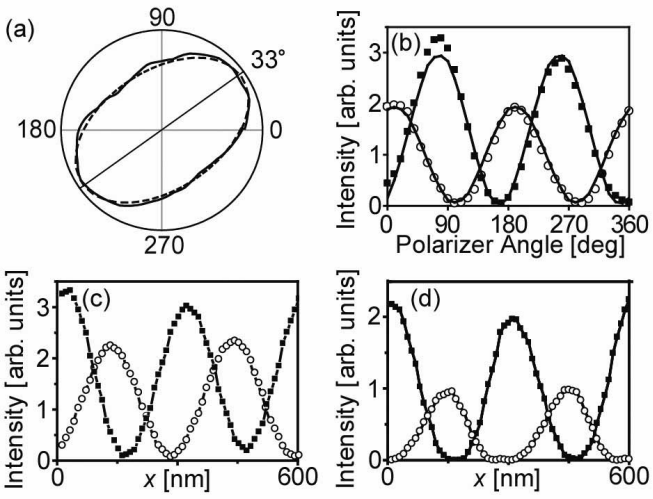

Fig. 5. (a). Far-field tip characterization: experimental (solid line) and fitted (dashed line) data, respectively. (b) Dependence of the scattered field intensity on the detecting polarizer angle at intensity maxima of $\left|E_{S,x}\right|^2$ (open circles) and $\left|E_{S,z}\right|^2$ (filled squares) of the standing wave generated on the prism surface. (c) Spatial variation of the intensity profiles for the detecting polarizer angles of 0° (open circles) and 90° (filled squares) as a function of the tip position. (d) Intensity profiles of $E_{Local,x}$ (open circles) and $E_{Local,z}$ (filled squares) field components obtained by applying the back-transformation to (c), using the experimentally measured polarizability tensor.

Finally, Fig. 6 shows the local field vectors of polarization obtained within a scan range of 600 nm on the prism surface obtained by using three different tips. The corresponding polarizability tensors are indicated above the vector plots. The results for Tip 1 and 2 are obtained with attached gold particles with a diameter of 200 nm [Fig. 4(b)] and 100 nm (not shown), respectively. In these cases the effective polarizability tensors are close to the identity matrix. The bottom one is obtained with the tip introduced in Fig. 5(a). For all three tips functionalized with gold nanoparticles of different size and shape, the measured local polarization vectors show a good agreement with the theoretical prediction Fig. 3(b), demonstrating the independence of the introduced vector mapping technique of local field polarization on the tip shape.

#85586 - $15.00 USD Received 23 Jul 2007; revised 5 Sep 2007; accepted 5 Sep 2007; published 29 Oct 2007

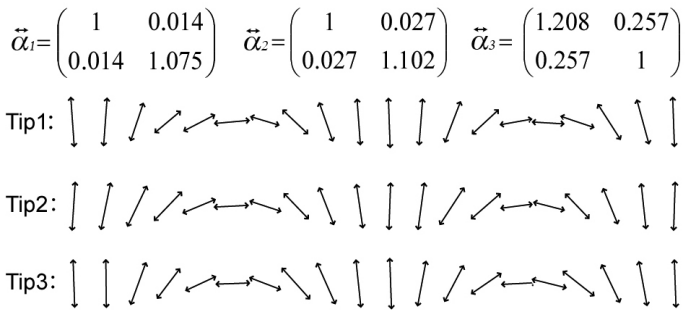

Fig. 6. Local field polarization vectors of the evanescent standing wave generated on the prism surface within a 600 nm scan range obtained by using three different gold-particle functionalized tips. The corresponding polarizability tensors are displayed above the scans.

4. Conclusion

We have studied on the tip shape dependence on the measured local field polarization vectors of evanescent standing waves generated on a prism surface when using gold nanoparticle functionalized tip as a local field scatter. The scattering geometry of the tip, i.e., the polarizability tensor, can be found by a far-field scattering measurement and the polarization state of the scattered light is determined by using a conventional ellipsometry technique, the RAE method. As far as the tip acts as an electric dipole scatterer, we could successfully reconstruct the local field polarization vectors independently of the particle size and shape. The reconstructed field polarization vectors match well with those expected for unperturbed evanescent surfaces waves. Generally one may expect a certain perturbation of the local electric field by the field scatterer. The demonstrated ability to quantitatively map electric field vectors of local polarization in simple cases, such as the standing surface waves investigated here, will certainly prove useful in obtaining a deeper understanding of the interaction between the tip scatterer and localized electric fields at surfaces. Experiments aimed at quantitatively probing these interactions are currently underway.

Acknowledgments

Research supports from the Korean government (Korean Science and Engineering Foundation Ministry of Science and Technology, Ministry of Commerce and Industry, Ministry of Education, and Research Council of the City of Seoul) and from the Deutsche Forschungsgemeinschaft (Priority research program SFB 296) are gratefully acknowledged.

#85586 - $15.00 USD Received 23 Jul 2007; revised 5 Sep 2007; accepted 5 Sep 2007; published 29 Oct 2007